Physics Letters B 747 (2015) 178–181

Contents lists available at ScienceDirect

Physics Letters B

www.elsevier.com/locate/physletb

Similarities between calculated scission-neutron properties and experimental data on prompt fission neutrons

N. Carjan [a,b,c,*], M. Rizea [b]

[a] Joint Institute for Nuclear Research, FLNR, 141980 Dubna, Moscow Region, Russia
[b] National Institute for Physics and Nuclear Engineering "Horia Hulubei", Str. Reactorului no. 30, P.O. BOX MG-6, Bucharest, Magurele, Romania
[c] CENBG, University of Bordeaux, 33175 Gradignan Cedex, France

ARTICLE INFO

Article history:
Received 1 February 2015
Accepted 19 May 2015
Available online 29 May 2015
Editor: J.-P. Blaizot

Keywords:
Scission neutrons
Prompt neutrons
Dynamical model
Angular distribution
Average energies
Neutron multiplicity

ABSTRACT

The main properties of the neutrons released during the neck rupture are calculated for ^{236}U in the frame of a dynamical scission model: the angular distribution with respect to the fission axis (on spheres of radii R = 30 and 40 fm and at time $T = 4 \times 10^{-21}$ s), the distribution of the average neutron energies (for durations of the neck rupture $\Delta T = 1$ and 2×10^{-22} s) and the total neutron multiplicity (for two values of the minimum neck-radius $r_{min} = 1.6$ and 1.9 fm). They are compared with measurements of prompt fission neutrons during ^{235}U(n_{th}, f). The experimental trends are qualitatively reproduced, i.e., the focusing of the neutrons along the fission axis, the preference of emission from the light fragment, the range, slope and average value of the neutron energy-spectrum and the average total neutron multiplicity.

1. Introduction

The emission of prompt fission neutrons (PFN) is essential in producing nuclear energy since it makes the chain reaction of fissile nuclei possible [1]. The theoretical and experimental study of their properties plays therefore an important role both in the fundamental understanding of the last stage of the fission process and in applications. The main characteristics of PFN (an emission along the fission axis and an exponential decreasing energy spectrum [2,3]) led to the first guess about their origin: they are evaporated by the fission fragments when these fragments are fully accelerated. As a result, we observe a kinematic anisotropy in the laboratory system that originates from an isotropic center of mass (c.m.) emission, the exponential spectrum simply reflecting the fragments' temperature.

The emission is therefore supposed to occur long after the division of the fissioning system into two fragments: it takes $\approx 10^{-20}$ s to reach 90% of TKE and $\approx 10^{-18}$ s to evaporate a neutron if the temperature is ≈ 1 MeV. Comparing to a typical nuclear (Fermi energy) time-scale ($\approx 10^{-22}$ s) these are very long times. One may expect another type of emission to occur before. Moreover, deviations from a standard evaporation spectrum [4–6] or from an isotropic emission in the c.m. [7,8] have been constantly detected. In spite of this, the evaporation hypothesis has never been questioned, its simplicity prevailing any counter argument.

The possibility of an earlier (e.g., around scission) neutron emission of a different origin, that could likewise explain the above mentioned PFN characteristics, was never brought up. However the existence of scission neutrons (SN) was not ignored [9] but they were usually invoked only to explain the deviations (in certain energy or angular domains) from the predictions of the evaporation theory. Such a procedure led obviously to the conclusion that SN represent a small fraction of PFN.

2. Nonadiabatic scission process

The most accepted mechanism for SN emission is the nonadiabatic coupling between the neutron degree of freedom and the rapidly changing neutron-nucleus potential during the scission process i.e., from the neck rupture at finite radius r_{min} to the absorption of the neck stubs by the fragments [10,11]. This idea was recently developed quantitatively in the frame of a quantum-mechanical microscopic model. At the beginning the sudden approximation was used [12–14] assuming the scission process to happen infinitely fast ($\Delta T = 0$). Then the time dependence was introduced through the time-dependent Schrödinger equation (TDSE) with time-dependent potential (TDP) [15,16]. This allows a short but finite transition time ($\Delta T \neq 0$) to be considered. Realistic

* Corresponding author.
E-mail address: carjan@in2p3.fr (N. Carjan).

http://dx.doi.org/10.1016/j.physletb.2015.05.050

values for ΔT are supposed to be around 10^{-22} s. The neutrons present in the fissioning nucleus just before scission evolve in time and quickly find themselves in a postscission potential where they are described by wave packets with some components in the continuum (hence partially released). In this paper we use these unbound parts of the neutron wave packets in order to estimate, for ^{236}U, the angular distribution of the SN with respect to the fission axis, the distribution of the SN average energies and the total SN multiplicity. These estimates are compared with PFN data collected in the thermal-neutron induced fission of ^{235}U.

3. Scission configurations

In our calculations the nuclear shapes just-before scission (two fragments connected by a thin neck) and immediately-after scission (two separated fragments) are described by Cassini ovals [17] with only one deformation parameter: $\alpha_i = 0.985$ (having $r_{min} = 1.6$ fm) and $\alpha_f = 1.001$ (having $d_{min} = 0.6$ fm) respectively. d_{min} is the distance between the surfaces of the two fragments along the z-axes. It is known that these ovals are very close to the conditional equilibrium shapes, obtained by minimization of the deformation energy at fixed value of the distance between the centers of mass of the future fragments [18,19]. To include asymmetric fission it is necessary to introduce a deviation from these ovals defined by a second parameter α_1 [20]. The chosen value of the minimum neck radius (1.6 fm) is slightly lower than predicted by the optimal scission shapes [21]. One can also deduce an approximate neck radius by general considerations like the size of the alpha particle. These theoretical estimates are ≈ 2 fm. Concerning d_{min} one expects to be larger when r_{min} is larger (the restoring forces being in this case stronger) but otherwise d_{min} is unknown.

4. Angular distribution of the unbound neutrons

Let us consider the neutron wave functions after scission (i.e. at $t = \Delta T$) $\hat{\Psi}^i$ (ΔT), that correspond at $t = 0$ to the eigenstates $\hat{\Psi}^i$ that are occupied in the initial configuration α_i. They are numerical solutions of TDSE with TDP obtained as in Refs. [15,16]. Their distribution over the eigenstates of the α_f configuration is given by

$$a_{if} = \langle \hat{\Psi}^i(\Delta T) | \hat{\Psi}^f \rangle. \tag{1}$$

Convention: a wave function that doesn't show a t-dependence is an eigenstate i.e., a solution of the stationary equation. All wave functions have an implicit dependence on the cylindical coordinates (ρ, z). a_{if} is $\neq 0$ only if $|\hat{\Psi}^i\rangle$ and $|\hat{\Psi}^f\rangle$ have the same projection Ω of the total angular momentum along the symmetry axis.

$f^i = |\hat{\Psi}^i_{em}(t)\rangle$, the emitted part of $|\hat{\Psi}^i(t)\rangle$, is given by the contribution of the unbound states to the wave packet:

$$|\hat{\Psi}^i_{em}(t)\rangle = |\hat{\Psi}^i(t)\rangle - \sum_{bound\ states} a_{if} |\hat{\Psi}^f\rangle$$

The corresponding current density weighted by the occupation probability v_i^2 of the respective state i:

$$\bar{D}_{em}(\rho, z) = \frac{i\hbar}{\mu} \sum_i v_i^2 (f^i \bar{\nabla} f^{i*} - f^{i*} \bar{\nabla} f^i), \tag{2}$$

provides the distribution of the average directions of motion of the unbound neutrons at any time t.

Here we assume that the fissioning system is in its lowest state at α_i which means a superfluid descent from saddle to just-before scission, i.e. to α_i defined by r_{min}. This is a good approximation in the case of spontaneous or sub-barrier fission [22–25], the partial pair-breaking taking place during the neck rupture.

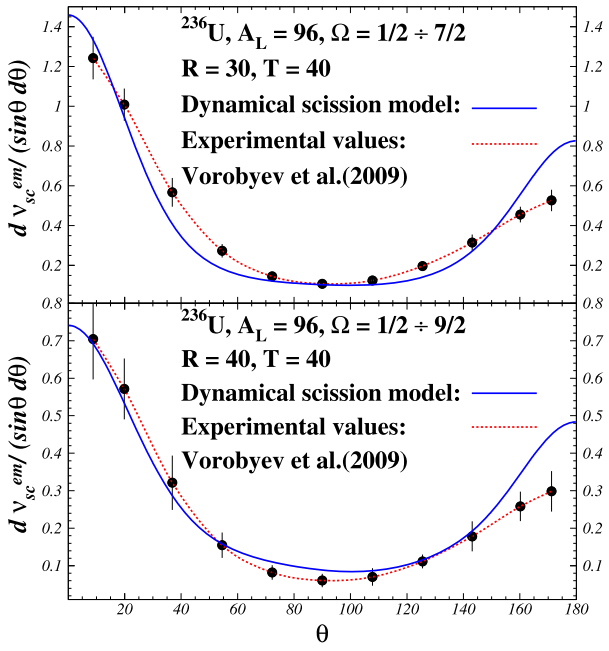

Fig. 1. Comparison between the angular distribution with respect to the fission axis calculated for SN and the one measured for PFN. Calculations are done for the most probable mass ratio $A_L = 96$ on two spheres of radii 30 fm (above) and 40 fm (below). The data points are normalized to the theoretical curve.

To calculate the angular distribution of the SN with respect to the fission axis one needs to integrate in time the radial component of $\bar{D}_{em}$ along the surface of a sphere of radius R containing the fissioning nucleus [26]:

$$d\nu_{sc}^{em}/(\sin\theta d\theta) = 4\pi \int_0^T \bar{D}_{em}(R, \theta, t) \bar{n}(R, \theta) R^2 dt. \tag{3}$$

$\bar{n}$ is the unit vector perpendicular to the surface. For R we choose 30 fm and 40 fm. In the calculations with $R = 40$ fm we also improved the Woods–Saxon potential at scission by replacing the gradient approximation [20] with an exact calculation of the distance to the nuclear surface. The upper limit of the time integral should be in principle ∞. In practice we can reach only a finite value $T = 4 \times 10^{-21}$ s.

The duration of the scission process ΔT is taken 10^{-22} s. During this short time the configuration of the scissioning nucleus is changing drastically from α_i to α_f. For $t > \Delta T$, in first approximation, we freeze the fragments at the configuration α_f since after scission (i.e., after α_f) the neutron motion is much faster than that of just-separated fragments. During this stage, i.e. from $t = \Delta T$ to T, the TDSE is solved neglecting the time dependence of the potential.

Eq. (3) is applied to the most probable mass division ($A_L = 96$) of ^{236}U. To compare with experimental data [27] (that were obtained with 16° angular resolution), the theoretical angular distribution, Eq. (3), has to be folded with the resolution function. The result is shown with solid line in Fig. 1. The resemblance with the measured trend is striking. Calculations with larger radius R and improved scission potential (presented in the lower part of the same figure) bring no significant change.

Table 1
Total number of SN released (ν_{sc}) (for $A_L = 96$ and $\Delta T = 1$) and number of neutrons (ν_{sc}^{em}) that crossed the spheres of $R = 30$ and 40 fm at succesive time intervals T. The ratio of the contributions from the L and H fragments is also included. All times are in 10^{-22} s.

A_L / ΔT	96 ($R = 30$)		96 ($R = 40$)	
	ν_{sc}	ν_L/ν_H	ν_{sc}	ν_L/ν_H
1	0.561	1.075	0.551	1.123
T	ν_{sc}^{em}	ν_L^{em}/ν_H^{em}	ν_{sc}^{em}	ν_L^{em}/ν_H^{em}
10	0.118	1.424	0.043	1.562
20	0.258	1.348	0.152	1.256
30	0.363	1.402	0.247	1.281
40	0.429	1.414	0.320	1.407

Even if the neutrons are released predominantly in the inter-fragment region [15,16], only few move perpendicular to the fission axis. Most of them are attracted (by the fragments, more by the light one) and focused along the fission axis as in the PFN experimental angular distribution.

The last five rows of Table 1 contain the calculated contributions of the L and of the H fragments to the SN multiplicity at different times T after scission. They represent neutrons that have crossed the sphere of radius R and move left and right to a plane at 90° to the fission axis. They are calculated by the integral of Eq. (3) with respect to the solid angle. A ratio ν_L^{em}/ν_H^{em} close to the experimental value (1.41) [28] is obtained. The first two rows contain neutrons that are left unbound at the end of the scission process calculated with Eq. (4). The contributions from the L- and H-fragments are estimated using the prescription from Ref. [14]. There is no information in ν_L and ν_H in which direction the neutrons are moving. Neutrons born in the H-fragment can move in the L-fragment direction.

5. Unbound-neutron multiplicity and average energy spectrum

The scission neutron multiplicity ν_{sc} is given by the sum of the probabilities P_{em}^i that a neutron occupying a given bound-state i is emitted:

$$P_{em}^i = v_i^2 \Big(\sum_f |a_{if}|^2\Big)$$
$$\nu_{sc} = 2\sum_i P_{em}^i \tag{4}$$

The i-sum is over bound states while the f-sum is over unbound states.

Due to the partial reabsorbtion of the neutrons by the fragments not all positive-energy states necessarily lead to unbound asymptotic states. It means that Eqs. (4) give only an upper limit. Although the inclusion of an imaginary potential will reduce the overall number of scission neutrons, the trends of their angular distribution (i.e., the focusing along the fission axis and the preference for the L-fragment direction) are kept.

Hence each neutron in the fissioning nucleus is released at scission (with probability P_{em}^i) and leaves the system during the acceleration of the fragments. Its average kinetic energy is:

$$E_n^i = \langle \hat{\Psi}_{em}^i(\Delta T)|\hat{\mathcal{H}}(\alpha_f)|\hat{\Psi}_{em}^i(\Delta T)\rangle. \tag{5}$$

$\hat{\mathcal{H}}$ is the single-particle Hamiltonian with extremely deformed Woods-Saxon mean field and related spin-orbit potential [15,16] at α_f.

The function $P_{em}^i(E_n^i)$ gives the distribution of the SN average energies. It is represented in Fig. 2 as a histogram. The experimental PFN spectrum [29] is also plotted to compare the trends: the slope, the range and the average value.

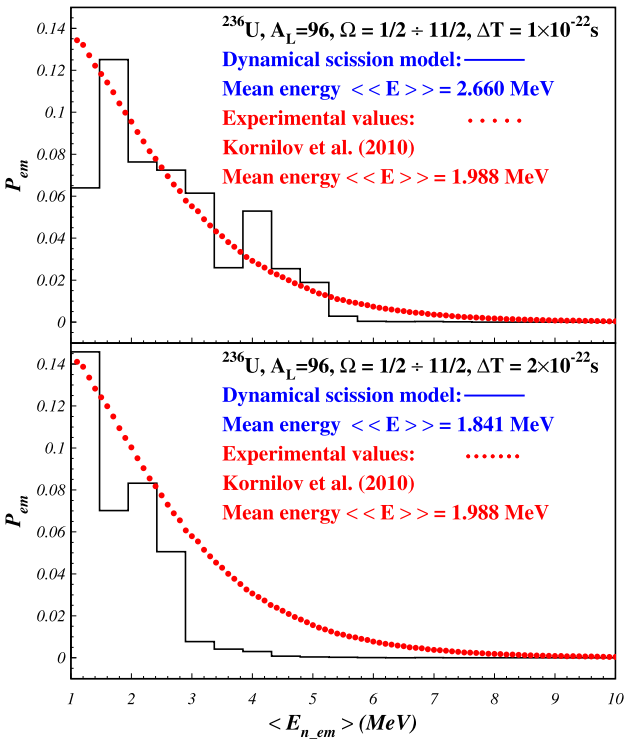

Fig. 2. Comparison between the histogram of the SN average energies calculated for the most probable mass division ($A_L = 96$) and the energy spectrum measured for all PFN. Calculations are performed for two transition times $\Delta T = 1$ (above) and 2 (below) $\times 10^{-22}$ s.

Table 2
Dependence of ν_{sc} (for $A_L = 96$) on (r_{min}, d_{min}) in fm and on ΔT.

ΔT / $r_{min}(d_{min})$	1.6 (0.6)	1.9 (2.0)
1×10^{-22} s	0.551	2.538
2×10^{-22} s	0.385	1.887

Although all SN are emitted by the same mechanism, their energies can be very different depending on the single-particle state they originate from. The average kinetic energies span a large interval from 1 MeV to more than 10 MeV with decreasing probabilities as in the PFN experimental spectrum.

For $\Delta T = 1 \times 10^{-22}$ s the average neutron energy $<< E_n >>=$ 2.7 MeV is larger than the experimental value (2.0 MeV [29]). For $\Delta T = 2 \times 10^{-22}$, $<< E_n >>= 1.84$ MeV, hence lower than the experimental value. Within the uncertainty of the transition time, one could therefore reproduce the average neutron energy.

Finally we study the dependence of the SN multiplicity, [Eq. (4)], on the scission configurations involved. The transition ($\alpha_i = 0.985 \rightarrow \alpha_f = 1.001$) that corresponds to $r_{min} = 1.6$ fm and $d_{min} = 0.6$ fm, used so far, is compared with the transition ($\alpha_i = 0.975 \rightarrow \alpha_f = 1.010$) corresponding to $r_{min} = 1.9$ fm (the theoretically predicted value [21]) and $d_{min} = 2.0$ fm. The results are presented in Table 2 for the most probable mass division ($A_L = 96$) and two transition times ΔT.

As expected, ν_{sc} decreases with increasing ΔT. If the collective motion is slow enough the transition is adiabatic ($\nu_{sc} = 0$) [15]. There is also a strong sensitivity of ν_{sc} on (r_{min}, d_{min}). One can see that the experimental value (2.41 [28]) can be reproduced with generally accepted values of r_{min} and ΔT.

One should add that the present mechanism through which neutrons are excited and eventually released during scission applies also to protons. However, due to their Coulomb repulsion,

protons are less present in the neck region where the potential varies at most and consequently they are less affected. In addition, the presence of the Coulomb barrier considerably hinders their emission.

6. Concluding remarks

The results of the calculation of the SN main observables are unexpected: these neutrons exhibit similar properties with the PFN measured in the reaction ($n_{th} + {}^{235}U$). We do not claim to have reproduced the PFN experimental data only with scission neutrons. Moreover, for a quantitative evaluation, the inclusion of an imaginary potential that will remove neutrons from the emission channel is necessary. However, since the currently accepted $\approx$ 10% contribution of SN to the total PFN multiplicity is based on the assumption that SN and neutrons evaporated from fully accelarated fragments have very different angular and energy distributions (that we demonstrated to be wrong), the amount of SN is in reality much larger.

Acknowledgements

Work partially supported by UEFISCDI Romania under the program PNII, contract IDEI 54/25.10.2011 and by PN09370102 of the Romanian Ministry of Education.

References

[1] H. Weigmann, in: C. Wagemans (Ed.), The Nuclear Fission Process, CRC Press, Boca Raton, USA, 1991, p. 63, Ch. 4.
[2] J.S. Fraser, Phys. Rev. 88 (1952) 536.
[3] H.-H. Knitter, U. Brosa, C. Butz-Jorgensen, in: C. Wagemans (Ed.), The Nuclear Fission Process, CRC Press, Boca Raton, USA, 1991, p. 497, Ch. 11.
[4] D.G. Madland, J.R. Nix, Nucl. Sci. Eng. 81 (1982) 213.
[5] O. Litaize, O. Serot, Phys. Rev. C 82 (2010) 054616.
[6] P. Talou, et al., Phys. Rev. C 83 (2011) 064612.
[7] K. Skarsvag, K. Bergheim, Nucl. Phys. 45 (1963) 72.
[8] A.S. Vorobyev, O.A. Scherbakov, et al., in: Proceedings XVII International Seminar on Interaction of Neutrons with Nuclei, Dubna, May 27–29, 2009, 2010, p. 60.
[9] G.A. Petrov, in: Proceedings of the Third International Workshop on Nuclear Fission and Fission-Product Spectroscopy, Cadarache, France, 11–14 May 2005, in: AIP Conf. Proc., vol. 798, 2005, p. 205.
[10] R.W. Fuller, Phys. Rev. 126 (1962) 684.
[11] I. Halpern, in: First Symposium on Physics and Chemistry of Fission, vol. II, IAEA, Vienna, 1965, p. 369.
[12] N. Carjan, P. Talou, O. Serot, Nucl. Phys. A 792 (2007) 102.
[13] N. Carjan, M. Rizea, Phys. Rev. C 82 (2010) 014617.
[14] N. Carjan, F.-J. Hambsch, M. Rizea, O. Serot, Phys. Rev. C 85 (2012) 044601.
[15] N. Carjan, M. Rizea, Int. J. Mod. Phys. E 21 (2012) 1250031.
[16] M. Rizea, N. Carjan, Nucl. Phys. A 909 (2013) 50.
[17] V.S. Stavinsky, N.S. Rabotnov, A.A. Seregin, Yad. Fiz. 7 (1968) 1051.
[18] V.M. Strutinsky, N.Ya. Lyashchenko, N.A. Popov, Nucl. Phys. 46 (1963) 639.
[19] A.A. Seregin, Yad. Fiz. 55 (1992) 2639.
[20] V. Pashkevich, Nucl. Phys. A 169 (1971) 275.
[21] F.A. Ivanyuk, K. Pomorski, Phys. Rev. C 79 (2009) 054327.
[22] H. Nifenecker, et al., in: Third Symposium of Physics and Chemistry of Fission, vol. II, Salzburg, IAEA, Vienna, 1965, p. 369.
[23] H.G. Borner, F. Gonnenwein, The Neutron: A Tool and an Object in Nuclear and Particle Physics, World Scientific, Singapore, 2012, Ch. 4.7.3.
[24] M. Rizea, N. Carjan, Phys. Proc. 31 (2012) 78.
[25] F. Ivanyuk, H. Hofmann, Nucl. Phys. A 657 (1999) 19.
[26] N. Carjan, M. Rizea, Nucl. Data Sheets 118 (2014) 199.
[27] A.S. Vorobyev, O.A. Scherbakov, et al., Nucl. Instrum. Methods A 589 (2009) 795.
[28] K. Nishio, et al., Nucl. Phys. A 632 (1998) 540.
[29] N. Kornilov, F.-J. Hambsch, et al., Nucl. Sci. Eng. 165 (2010) 117.